Clim. Past, 22, 505–516, 2026
https://doi.org/10.5194/cp-22-505-2026
© Author(s) 2026. This work is distributed under
the Creative Commons Attribution 4.0 License.

Climate of the Past
Open Access
EGU

Role of paleogeography on large-scale circulation during the early Eocene

Fanni Dóra Kelemen[1], **Richard Lohmann**[1], **Jiang Zhu**[2], **and Bodo Ahrens**[1]

[1]Institute for Atmospheric and Environmental Sciences, Goethe University Frankfurt, Frankfurt am Main, Germany
[2]NSF National Center for Atmospheric Research, Boulder, Colorado, USA

Correspondence: Fanni Dóra Kelemen (kelemen@iau.uni-frankfurt.de)

Received: 4 October 2025 – Discussion started: 15 October 2025
Revised: 28 January 2026 – Accepted: 17 February 2026 – Published: 5 March 2026

Abstract. The configuration of continents and oceans has a major influence on Earth's climate by shaping large-scale atmospheric circulation patterns. In this study, we investigate the effect of early Eocene paleogeography, specifically from the Ypresian stage, on extratropical eddies. In our analysis we highlight the influence of the epicontinental West Siberian Sea as well as the impact of the lack of the Antarctic Circumpolar Current on mid-latitude cyclones and blocking events. Previous work from the Deep-Time Model Intercomparison Project (DeepMIP) has shown changes in atmospheric eddy heat transport under early Eocene boundary conditions. This motivates our analyse of mid-latitude cyclones and blocking events under early Eocene boundary conditions. For the analysis we use six-hourly output from an atmosphere-only CESM1.2 simulation, which is an extension of the corresponding DeepMIP $1 \times CO_2$ experiment. In our simulation, cyclonic activity strengthens at the northern mid-latitudes and weakens at the southern mid-latitudes under early Eocene boundary conditions compared to pre-industrial. Moreover, the blocking signal, which is dominated by the northern hemisphere under pre-industrial conditions, becomes less pronounced. Our results show that, through air–sea interactions the paleogeographic features of the early Eocene produce a more balanced heat transport between the hemispheres and atmospheric processes compared to pre-industrial conditions.

1 Introduction

The arrangement of continents and oceans has an important effect on climate, from regional to global scales. Throughout Earth's history, paleogeography has shaped key aspects of the climate system, including oceanic and atmospheric circulation, and the carbon cycle. An example in the ocean is the Antarctic Circumpolar Current (ACC), which could only develop after ocean passages opened 30 million years ago (Scher et al., 2015). The continental configuration also influences atmospheric circulation. It has been shown (Agustsdottir et al., 1999) that through the geological time scale, paleogeography plays the most important role in influencing winter storm distribution. Also, monsoonal circulation is shown to be dependent on the continental configuration. For example, continents with a C-shape land distribution at the tropics, two continental landmasses at the two sides of the Equator connected with a bridging land, favours monsoon development (Mei et al., 2025). In an other aspect, when the majority of continents are located at the tropics and experience tropical precipitation, silicate weathering can effectively remove CO_2 from the atmosphere inducing a cooling and ice accumulation (Ramstein, 2011). Thus, tectonic changes have the capacity to trigger ice ages, through their influence on the carbon cycle. In paleoclimate research, attributing different forcing mechanisms is essential for understanding climate dynamics and for making conclusions transferable to also future scenarios. Moreover, studying past warm climates are of high relevance because of their information on how our climate system worked under high CO_2 concentrations.

Here, we consider the role of the early Eocene paleogeography on large-scale circulation patterns. The time pe-

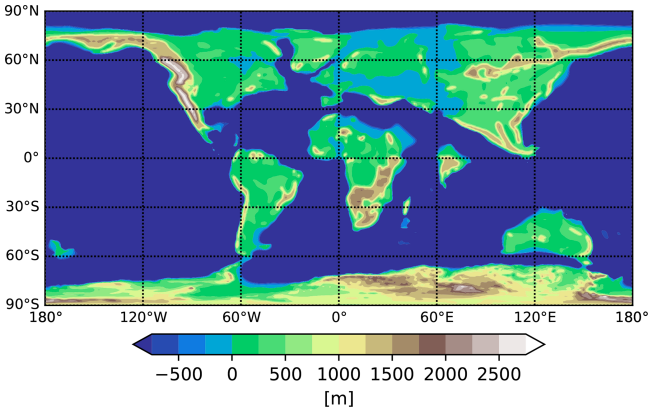

Figure 1. Early Eocene paleogeography from Herold et al. (2014).

riod we focus on is the Early Eocene Climatic Optimum (EECO, ∼ 53–51 Ma), which is characterised by exceptional warmth (approximately 10–16 °C warmer than pre-industrial climate) (Inglis et al., 2020), low meridional temperature gradients (Evans et al., 2018) and high CO_2 concentrations (around 1600 ppm) (Cenozoic CO_2 Proxy Integration Project (CenCO2PIP) Consortium et al., 2023). There has been coordinated effort amongst modelling and proxy groups, under the initiative known as the Deep-Time Model Intercomparison Project (DeepMIP), to increase our understanding of this period in Earth climate history (Lunt et al., 2021). In our study, we consider the paleogeography used in the first phase of DeepMIP, from the early Eocene, the Ypresian stage representing the Earth between ∼ 55 to ∼ 50 Ma (see Fig. 1) (Lunt et al., 2017; Herold et al., 2014).

The most notable features of this early Eocene paleogeography are the wider Pacific Basin and thus narrower Atlantic Ocean, the tropical location of the Indian subcontinent and the lack of the Himalayas. Moreover, an important characteristic in the Northern Hemisphere is the connection between the Arctic and the Tethys Ocean through the shallow West-Siberian Sea (Shellito et al., 2009; Wang, 2004). During the early Eocene there were no currents connecting the Arctic to the Pacific basin, as the Bering Strait was closed, thus oceanic heat transport from the tropics to the Arctic flow through the West Siberian Sea (Akhmetiev et al., 2012). This is underlined by proxy records showing that the mean annual sea surface temperature in the Arctic Ocean and the West-Siberian Sea was very similar and at least 20 °C (Frieling et al., 2014). In the Southern Hemisphere, the location of the Antarctic continent was very similar to modern conditions, but both Australia and South America were located more to the south, causing the Drake Passage and the Tasman Gateway to be narrow and shallow, i.e. oceanographically closed (negligible water, heat or mass transport through it) (Herold et al., 2014) and thus inhibiting the development of the ACC.

Previous analysis of the DeepMIP ensemble investigated the effects of CO_2 and non-CO_2 boundary conditions (paleogeography, lack of ice sheets, vegetation, rivers) on meridional heat transport (MHT) processes (Kelemen et al., 2023). The study showed that in the model simulations the total MHT does not change much due to the early Eocene non-CO_2 boundary conditions. Nevertheless, there are changes in the atmospheric heat transport (AHT), and in the ocean heat transport (OHT) (Fig. 2a). The AHT shifts slightly toward the northern hemisphere and the OHT shifts towards the southern hemisphere. The later one is likely related to the fact that, in most DeepMIP models' deep-water formation occurs in the Southern Ocean (Zhang et al., 2022). Thus, due to the change in deep-water formation, respective to modern days, the hemispheric distribution of OHT changes as well. Kelemen et al. (2023) also showed that the partitions of AHT, namely the heat transport through different physical processes such as the atmospheric meridional overturning circulation (MOC), the stationary (SE) and the transient eddies (TE), also change due to the non-CO_2 paleo boundary conditions. Most notable is the increase in TE heat transport at the northern mid-latitudes, and the compensating decrease in SE heat transport (Fig. 2b). Meanwhile, over the southern mid-latitudes, a decrease in TE heat transport is identified in the data (Fig. 2b), which is not compensated by other processes, thus mainly responsible for the decrease in AHT over the Southern Hemisphere. The Southern Hemispheric AHT decrease is also linked to the aforementioned increase in OHT, consistent with the Bjerknes compensation mechanism.

In this study, we further investigate the changes seen in the heat transport analysis (Kelemen et al., 2023), and analyze how the non-CO_2 paleo boundary conditions, most notably the early Eocene paleogeography, influences large-scale circulation patterns, especially at the mid-latitudes where AHT and its differences are maximal. We are focusing primarily on mid-latitude circulations patters, cyclones and blockings. For the analysis we use data from CESM1.2 model simulations, which are the extensions of the DeepMIP simulations (Zhu et al., 2019; Lunt et al., 2021).

Our goals in this paper are:

1. To understand the early Eocene global circulation and climate. The better understanding of large-scale circulation patterns and their changes related to paleogeography helps the interpretation of proxy records.

2. To demonstrate how AHT change materialises through dynamical processes, and to show how surface interactions govern large-scale atmospheric circulation patterns.

This paper is structured as follows. In Sect. 2, we introduce the climate model simulations and the identifying algorithms for cyclones and blockings. In Sect. 3, we provide an overview of our results considering the Northern and Southern Hemisphere. In Sect. 4, we discuss our findings and the

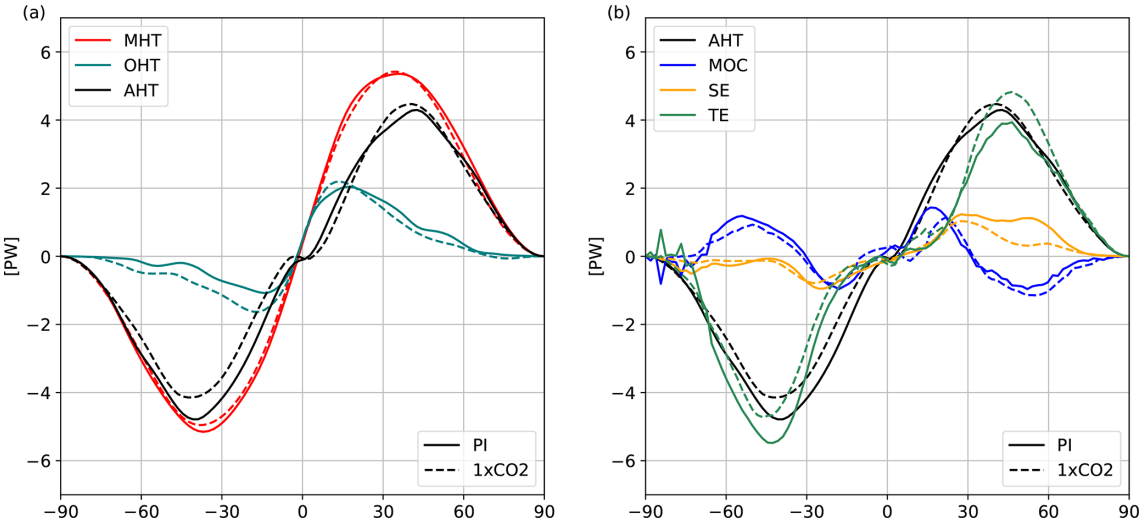

Figure 2. Annual meridional heat transport (MHT) and its partitions from the DeepMIP based CESM1.2 pre-industrial (solid) and $1 \times CO_2$ (dashed) simulations. **(a)** MHT divided into atmospheric (AHT) and oceanic (OHT) heat transport, **(b)** AHT divided into meridional overturning circulation (MOC), stationary eddies (SE) and transient eddies (TE) for further details on the calculations see Kelemen et al. (2023).

wider context of the dynamic changes and finish with a summary and our conclusions.

2 Data and Methods

2.1 Climate Model Data

The study uses the Community Earth System Model version 1.2 (CESM) in an atmosphere-only configuration, where the atmosphere and land modules are active and have a horizontal resolution of $1.9° \times 2.5°$ (latitude $\times$ longitude) with 30 hybrid sigma-pressure levels in the atmosphere. The ocean is taken into consideration through prescribed monthly Sea Surface Temperature (SST) and sea-ice extent. For other details on the model and boundary conditions, see Zhu et al. (2019) and Lunt et al. (2021). For our analysis, we utilised two simulations; a pre-industrial control simulation and a $1 \times CO_2$ EECO experiment, where all boundary conditions are changed to represent the EECO conditions, except for the CO_2 concentration, which is kept at the pre-industrial level. The differences between the modern and EECO simulation are the changes in paleogeography, the lack of ice sheets, vegetation, aerosols and rivers. Thus, comparison of these simulations reveals the effect of these boundary conditions, with paleogeography hypothesized to make the largest contribution.

The simulations were extended from the corresponding coupled simulations in the DeepMIP ensemble (Lunt et al., 2021). The motivation for the extension is the need for at least 6 hourly resolution to enable direct cyclone tracking, which is not possible in the original DeepMIP dataset's monthly data. The atmosphere-only configuration was sufficient for our study, as we are focusing on atmospheric processes, and do not expect the ocean, which reached equilibrium in the DeepMIP simulation, to change notably in the timeline of our relatively short simulations. The atmospheric initial conditions were taken from the final state of the DeepMIP simulations, thus the simulations were direct continuations of the DeepMIP simulations in the atmosphere, which made spin up unnecessary. The ocean boundary conditions were monthly SST as well as sea ice fraction mean values from the last 100 years of the DeepMIP simulations. Our simulations were integrated for 30 model years to represent the climatology of the climate state.

2.2 Cyclone Tracking

To identify cyclones in the simulations, we adapted the cyclone tracking algorithm of Kelemen et al. (2015) for the global field. The algorithm identifies cyclones as mean sea level pressure minima and connects the pressure centres in time by a nearest neighbour approach.

For the climatological analysis we do not consider the trajectories one-by-one, but calculate a track density field from them. The track density field represents the average number of cyclone centre passing through each model grid point per year or per season. The field is calculated through the cyclone centres, thus the area where cyclones affect the climate is larger and surrounds the high track density storm tracks. To focus on the significant transient eddies, our analysis includes only cyclones that persist for more than one day, travel at least 1000 km, and exhibit a pressure minimum at least 20 hPa below the global mean pressure. This filters out weak stationary pressure minima, which are often connected to orography, and ensures that we are detecting deep tran-

sient eddies which transport heat from the subtopics to the polar regions.

2.3 Blocking calculation

The hybrid blocking index evaluates the geopotential height at 500 hPa. It combines an anomaly approach with a gradient approach as described in Lohmann et al. (2024): geopotential height anomalies must exceed the climatological mean by one standard deviation to be counted as instantaneous block. To focus on persistent blocking systems, instantaneous blocks were counted as block if a minimum duration of 5 days and a minimum spatial extent of 15° in longitude and 1.5×10^6 km^2 was fulfilled. Details of the algorithm are described in the appendix. For the climatological analysis, we calculated the mean blocking frequency defined as the percentage of days with block compared to the total number of days.

3 Results

The analysis of the cyclone tracks shows a change in spatial pattern in both Hemispheres between the pre-industrial and the $1 \times CO_2$ simulations (Fig. 3). Under pre-industrial conditions, mid-latitude cyclones in the Northern Hemisphere are concentrated around two distinct areas over the Pacific and Atlantic Oceans (Fig. 3a). On the other hand, Southern Hemisphere cyclone tracks distribute around Antarctica in a O shape (Fig. 3c). However, under early Eocene conditions, the spatial distribution of cyclone tracks becomes more balanced as the distinction between the Pacific and Atlantic paths becomes less pronounced (Fig. 3b). Also, there is an increase in cyclone tracks passing over land areas, especially over Europe. In contrast, in the Southern Hemisphere there are fewer cyclone tracks under early Eocene conditions compared to pre-industrial, and the track climatology shows several small density centres around Antarctica (Fig. 3d), which is due to the more fragmented Southern Ocean basin. These changes are also reflected in the number of cyclones (Fig. 4), with an average annual increase of 36 % in the Northern Hemisphere and a decrease of 32 % in the Southern Hemisphere. This makes the cyclone distribution between the hemispheres more balanced, although the average annual cyclone number is still higher in the south than in the north. Moreover, there is a decrease in the annual cyclone number globally under early Eocene conditions compared to pre-industrial. The changes are consistent through all seasons, but most prominent during each hemisphere's winter and spring season. The heat, transported by the mid-latitude cyclones, is what we call transient eddy heat transport in the heat transport analysis. Thus these findings are in line with the increased transient eddy heat transport in the northern mid-latitudes and the decreased transient eddy heat transport in the southern mid-latitudes, respectively (Fig. 2).

Early Eocene blocking frequencies in the northern mid-latitudes show a general decrease and a shift from modern Europe to the east to the West-Siberian Sea (Fig. 5a and b). This is also in line with the heat transport analysis, showing a decrease in the stationary eddy heat transport at the northern mid-latitudes (see Fig. 2). The eastward shift of blocking frequency is in line with the eastward shift of the cyclone tracks to the West-Siberian Sea since the eastern boundary of cyclone tracks is a common region of blocking formation. The heat transport analysis does not show large changes in the stationary eddy heat transport at the southern mid-latitudes, which is reflected in the visually similar blocking frequencies in the early Eocene and in the pre-industrial period (Fig. 5c and d). Nevertheless, in the early Eocene the southern blockings have a more dispersed spatial distribution around Antarctica than in the pre-industrial climate.

Mid-latitude cyclones play a key role in the hydroclimate as they transport moisture and are associated with a large portion of extratropical precipitation. They generally produce more precipitation over oceanic regions than over land due to greater moisture availability. Moreover, enhanced precipitation also occurs when mid-latitude cyclones encounter orographic barriers, and orographic lifting takes place. For qualitative measure we plotted boreal winter (December, January and February) and southern winter (June, July and August) cyclone track densities along the respective seasonal precipitation fields (Figs. 6 and 7). In the Northern Hemisphere, cyclones are more prominent during winter and they precipitate along the Tethys Ocean and the West-Siberian Sea, bringing moisture to an area which is dryer under modern conditions. Moreover, during the early Eocene the west coast of North America is experiencing high precipitations, which is probably due to a combination of the higher number of cyclone tracks in the region and the cyclones' interaction with orography. In the Southern Hemisphere the most cyclones occure during the southern winter (see Fig. 4) and they bring precipitation to the western coast of Australia and South America (Fig. 7). Both of these regions are located souther in the early Eocene topography than in modern times, thus more in the paths of the mid-latitude cyclones.

4 Discussion and Conclusions

The meridional heat transport analysis identified three main characteristics (Fig. 2) when comparing the pre-industrial and $1 \times CO_2$ Eocene simulations:

- increase of transient eddy heat transport at the northern mid-latitudes
- decrease of stationary eddy heat transport at northern mid-latitudes
- decrease of transient eddy (and atmospheric) heat transport at southern mid-latitudes

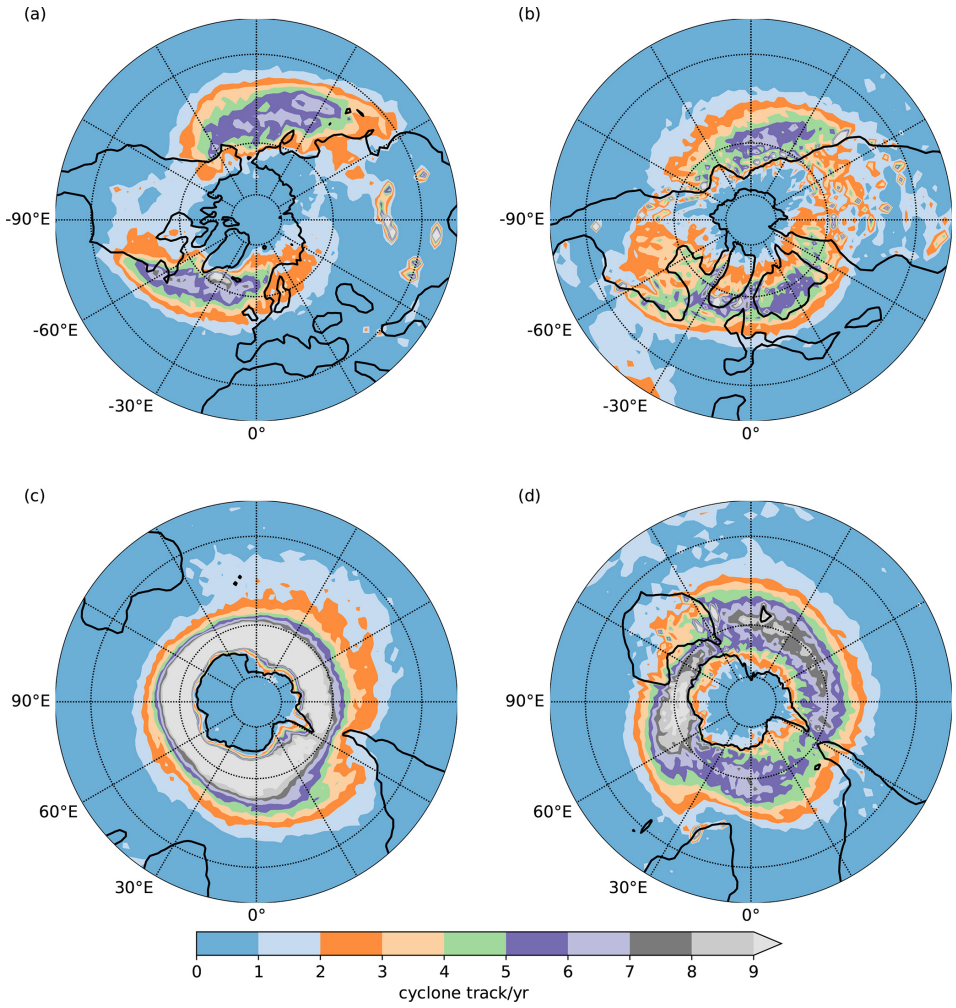

Figure 3. Global annual mean track density under pre-industrial **(a, c)** and early Eocene ($1 \times CO_2$) **(b, d)** conditions.

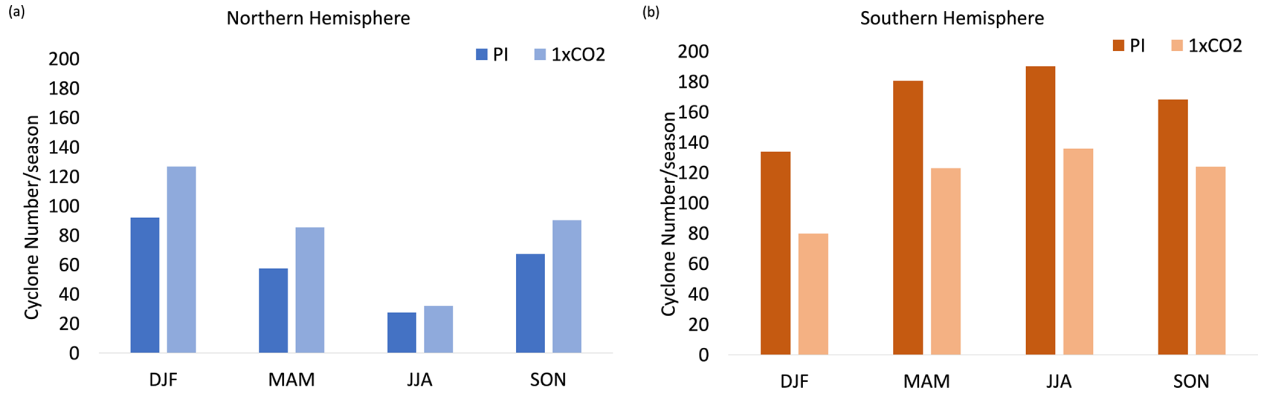

Figure 4. Seasonal distribution of cyclone numbers in the pre-industrial and early Eocene ($1 \times CO_2$) simulations over the **(a)** Northern Hemisphere, **(b)** Southern Hemisphere.

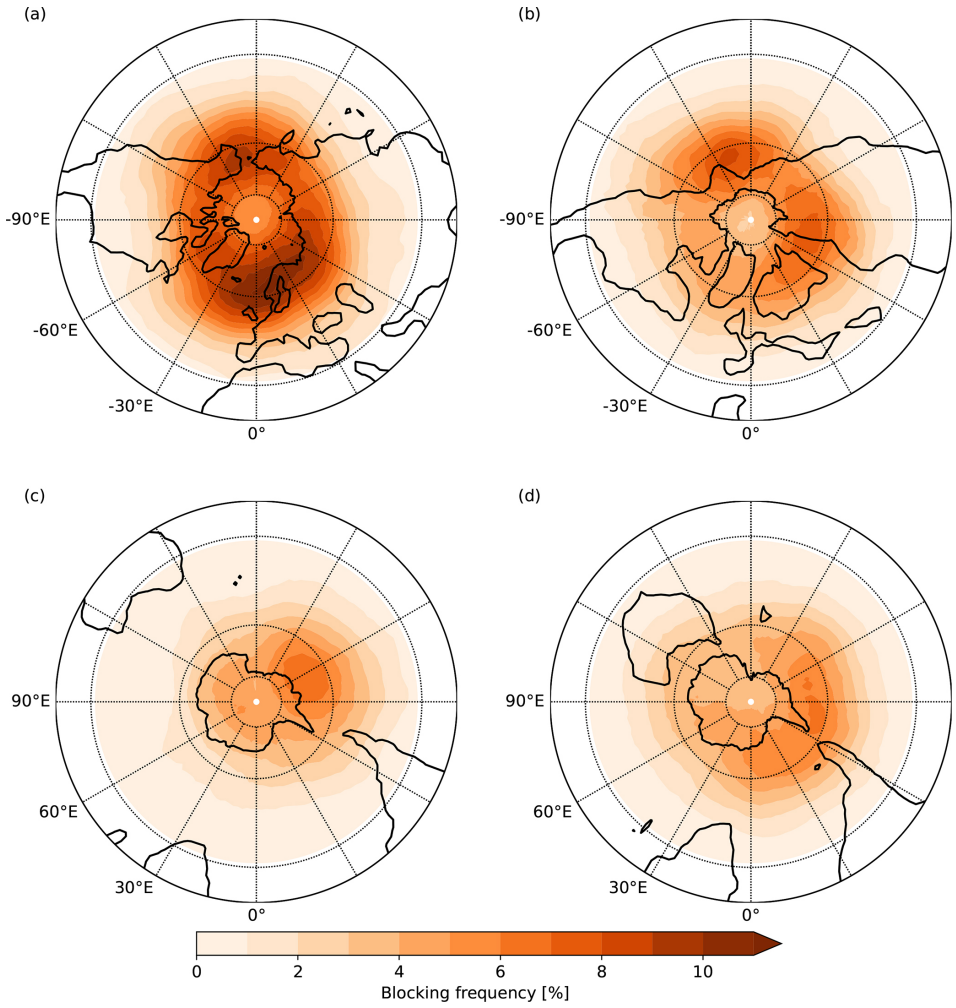

Figure 5. Annual mean blocking frequency under pre-industrial **(a, c)** and early Eocene ($1 \times CO_2$) **(b, d)** conditions.

These characteristics are due to the paleo boundary conditions, most notably the different configuration of continents and their orography. The cyclone and blocking analysis showed that the increase of transient eddy transport over the northern mid-latitudes is due to the increase in cyclone numbers, the decrease of stationary eddy transport is due to less frequent blockings at the northern mid-latitudes. Moreover, the southern mid-latitude transient eddy heat transport decrease is connected to the decrease of cyclone numbers. This change in the Southern Hemisphere is not compensated by other processes in the atmosphere, thus effects the AHT. Nevertheless, it is compensated by the OHT through the Bjerknes compensation. Thus, the total MHT remains very similar in the pre-industrial and $1 \times CO_2$ Eocene simulations.

The changes in paleogeography influence the air-sea interactions in the climate system. In the Northern Hemisphere, the Tethys Ocean and the West Siberian Sea served as additional sources of heat and moisture. This effect was especially pronounced during winter, when the thermal contrast between the epicontinental West Siberian Sea and the neighbouring land areas of Europe and Asia was highest. Comparing the latent and sensible heat fluxes over the Eurasian region reveals that over the West Siberian Sea the two fluxes are of comparable magnitude, thus the Western Siberian Sea enhances thermal contrast and act as a moisture source, whereas over the Tethys Ocean the surface energy exchange is dominated by latent heat flux (Fig. 8). This configuration enhances baroclinic instability in this region, which we saw as an increase in cyclone numbers.

In the Southern Hemisphere, the most significant changes in paleogeography compared to modern are the nearly closed Drake Passage and Tasman Gateway. These two narrow and shallow straights prevented the development of the wind driven circumpolar ocean current around Antarctica, the Antarctic Circumpolar Current (ACC). The wind field at the lowest model level, which is following the surface, is indeed weaker in the $1 \times CO_2$ Eocene simulation than under modern circumstances (Fig. 9a and b). Under pre-industrial conditions the ACC is crucial in maintaining the strong oceanic

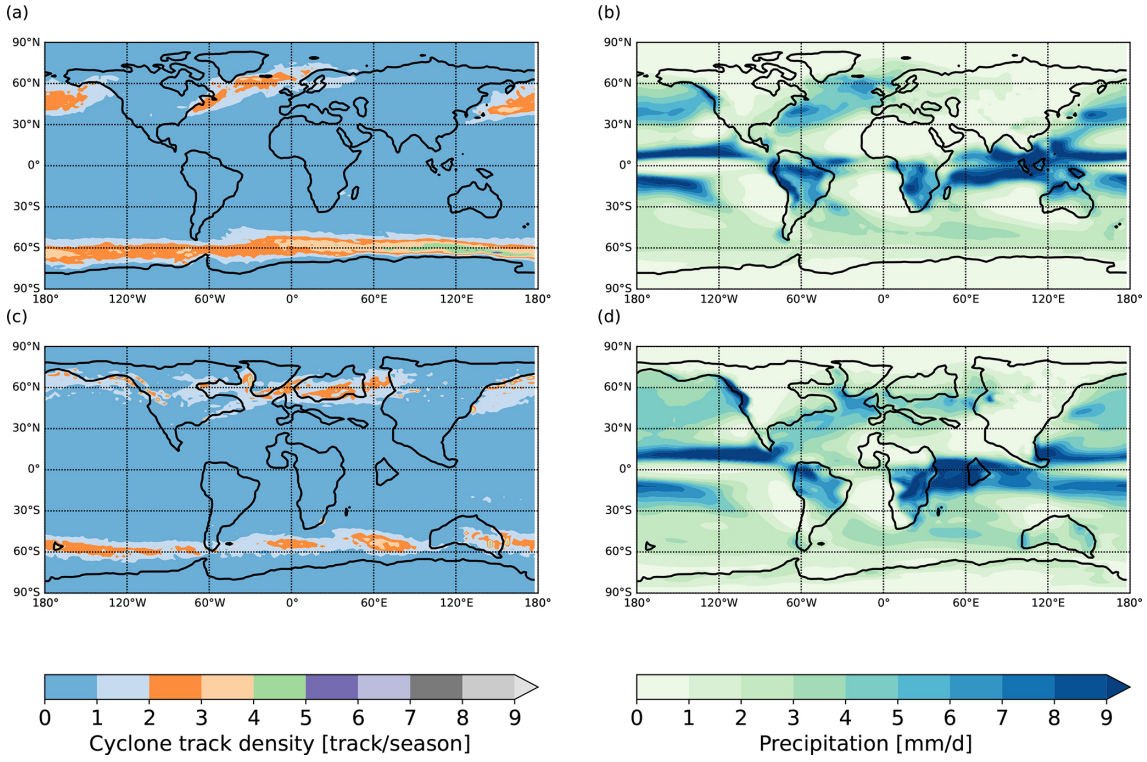

Figure 6. Boreal winter (DJF) track density **(a, c)** and mean precipitation **(b, d)** in the **(a, b)** pre-industrial and **(c, d)** early Eocene ($1 \times CO_2$) simulations.

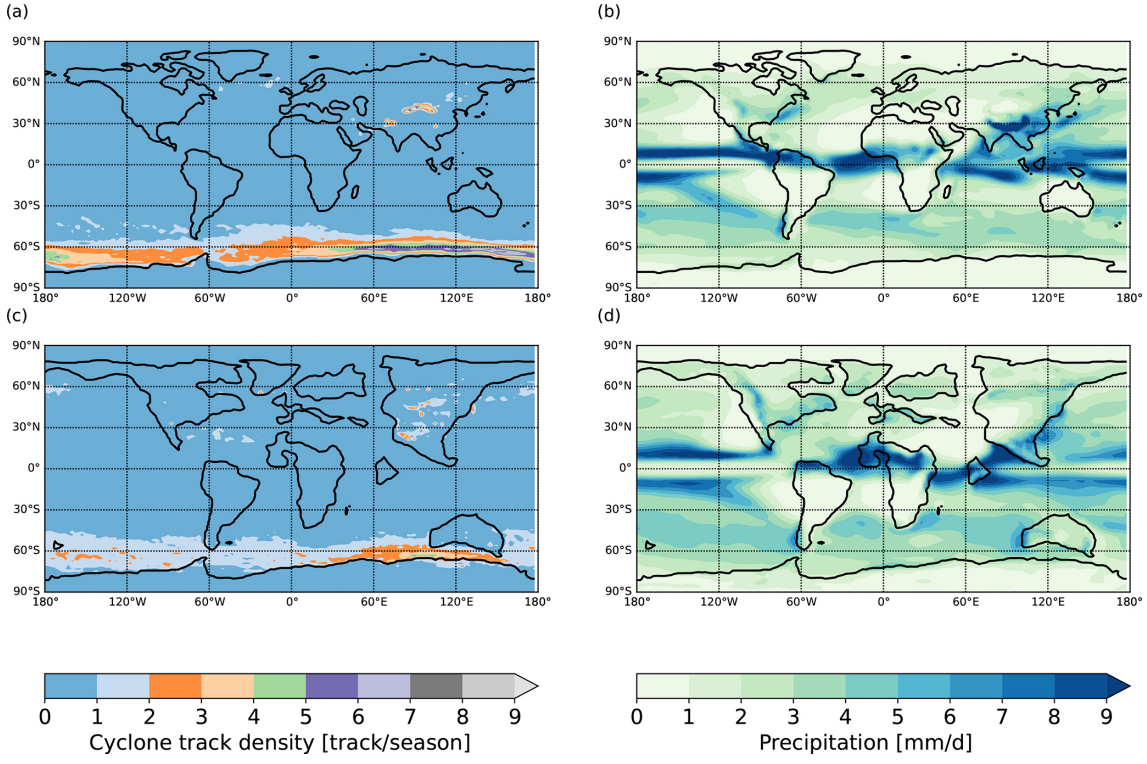

Figure 7. Southern winter (JJA) track density **(a, c)** and mean precipitation **(b, d)** in the **(a, b)** pre-industrial and **(c, d)** early Eocene ($1 \times CO_2$) simulations.

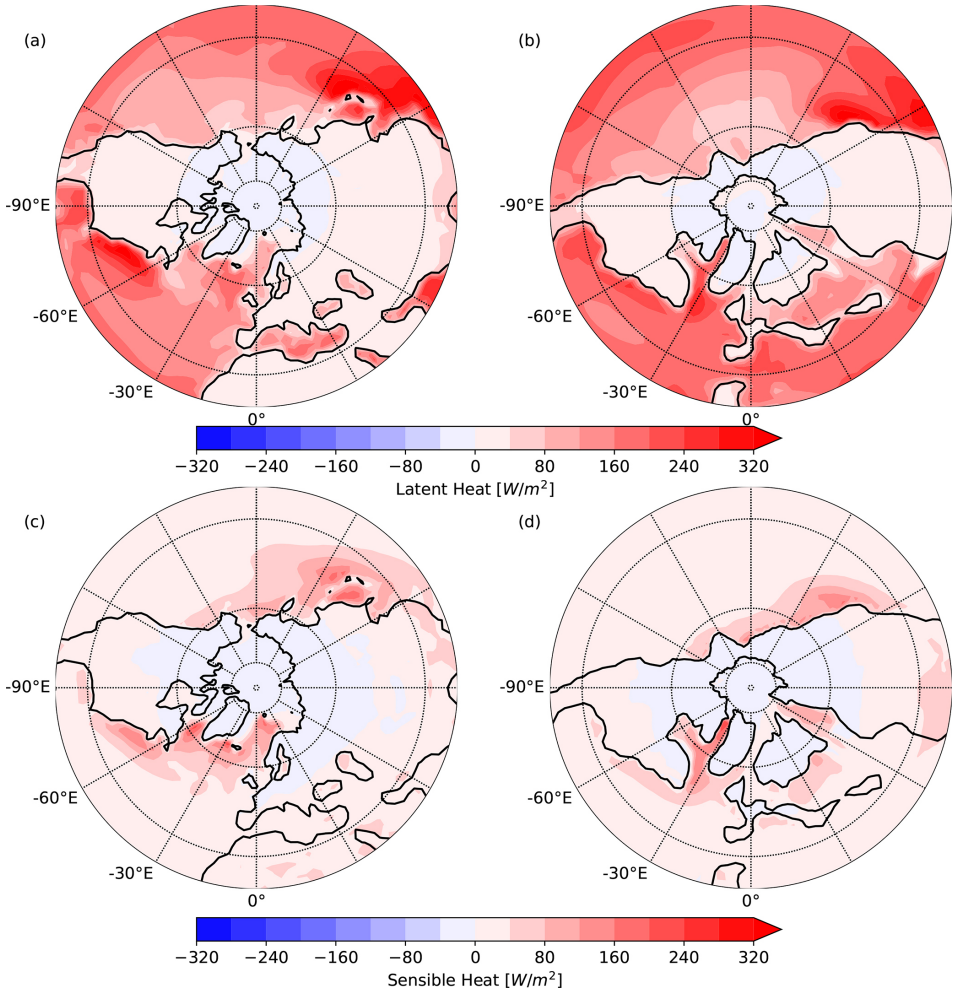

Figure 8. Latent heat **(a, b)** and sensible heat **(c, d)** fluxes during boreal winter over the Northern Hemisphere in the pre-industrial **(a, c)** and early Eocene ($1 \times CO_2$) **(b, d)** simulations.

temperature gradient between cold polar and warmer subtropical waters. This, in turn, enhances meridional temperature gradients in the lower atmosphere, which, through the thermal wind relationship, increases baroclinic instability, the fuel of mid-latitude cyclones. Under early Eocene conditions, without the ACC, the baroclinic instability decreases in the region, which is also evident by the weaker Southern Hemispheric jet stream (Fig. 9c and d). Overall, the ACC is dynamically connected to the Southern Hemispheric mid-latitude cyclones, and its absence in the $1 \times CO_2$ Eocene simulation is in line with the fewer cyclone number in the region (Fig. 4). Shaw et al. (2022) showed that in modern climate the Southern Hemispheric jet stream is stronger than its northern counterpart, and the Southern Hemisphere is stormier. In our results, we found that under early Eocene conditions the signal between the hemispheres are more balanced, due to the increase in Northern Hemispheric storms and the decrease in Southern Hemispheric storms.

We conclude that through air-sea interactions, the paleogeography notably influences atmospheric large-scale circulation patterns. Under early Eocene circumstances, this influence meant increased mid-latitude baroclinity over the Northern, but decresed baroclinicity over the Southern Hemisphere, which results in a more balanced heat transport among hemispheres and atmospheric processes than in the pre-industrial climate. In the Northern Hemisphere, the increased baroclinic instability resulted in increased heat transport by large eddies, nevertheless this process seems to be compensated by less heat transport via blocking systems. On the other hand, in the Southern Hemisphere the decreased baroclinity and thus less heat transport via mid-latitude cyclones is not compensated by other processes in the atmosphere. The net effect of paleogeography related changes on AHT, is a shift towards the Northern Hemisphere, which is, in turn, compensated by a southward shift in OHT. This increase in southward OHT is connected to the southern deep-water formation under early Eocene paleo boundary condi-

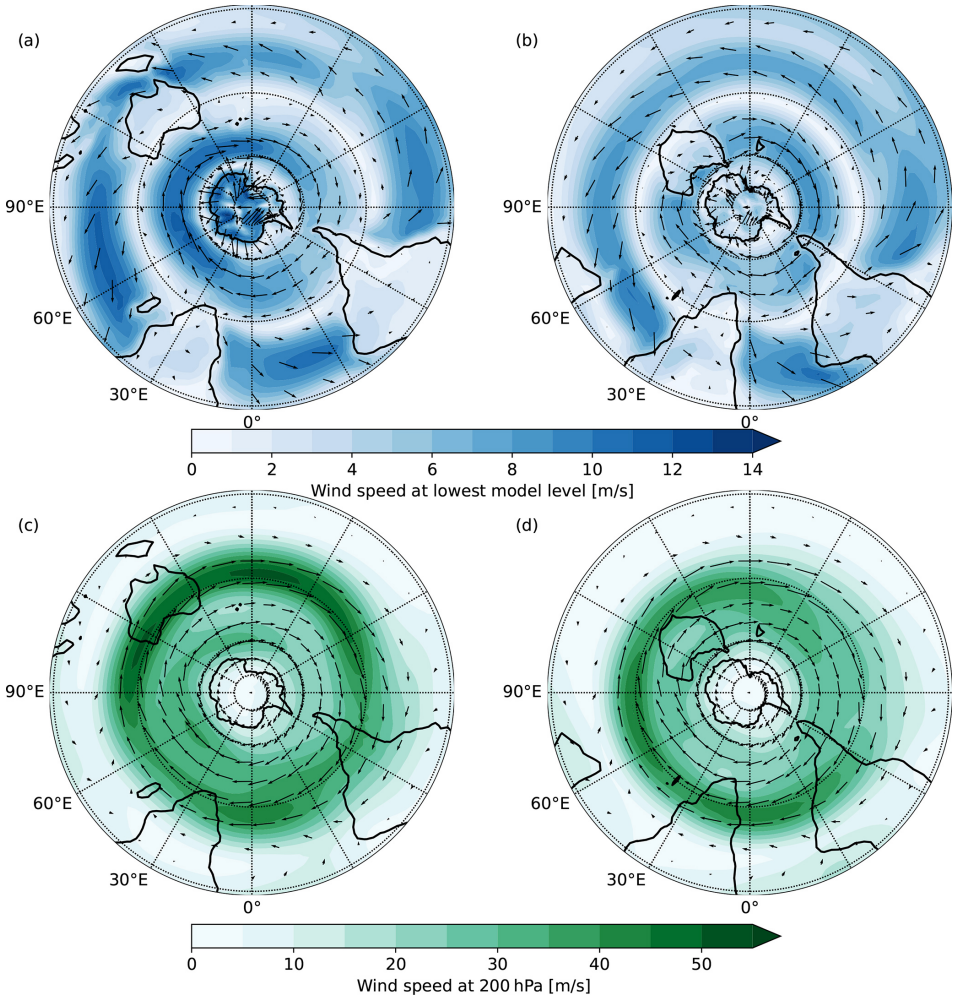

Figure 9. Horizontal wind at lowest model level **(a, b)** and at 200 hPa **(c, d)** during southern winter (JJA) over the Southern Hemisphere in the pre-industrial **(a, c)** and early Eocene ($1 \times CO_2$) **(b, d)** simulations.

tions (Zhang et al., 2022; Kelemen et al., 2023). The compensation is needed, because from the energetic perspective, a change in AHT needs to be compensated by the OHT to fulfil the top of the atmosphere energetic constraint on MHT. Thus, under the early Eocene conditions due to the AHT changes, the ocean needs to increase its heat transport over the Southern Hemisphere, which favours the development of a Southern Hemisphere-driven overturning circulation (Zhang et al., 2022).

This study shows that the early Eocene paleogeography affects atmospheric large scale processes and ocean circulation both in a direct and indirect way. For the ocean, the direct effects consist of strait geometry, and the indirect effects include the heat transport processes' influence on deep-water formation. Our results support the hypothesis that under early Eocene boundary conditions the Southern Ocean deep-water formation is more likely to fulfil the energetic constraints of the climate system.

In this paper, we investigated the role of early Eocene orography on large scale circulation patterns. We compared atmosphere only CESM model simulations describing pre-industrial conditions and modern day orography versus $1 \times CO_2$ simulations containing early Eocene boundary conditions including paleogeography, the lack of ice sheets, different vegetation and rivers. For ocean boundary conditions, we used the SST values form DeepMIP CESM simulations. Our research was motivated by a meridional heat transport analysis, which showed changes in the heat transport of transient eddies (cyclones) and stationary eddies (blockings) at the mid-latitudes. We found that the increase in transient eddy transport in the northern mid-latitudes is connected to the increase in cyclone numbers. In the early Eocene continental configuration, the presence of the warm and shallow epicontinental West Siberian Sea enhances air-sea interactions and acts as an extra heat and moisture source, which increases the baroclinic instability in the region. The change in cyclone numbers and paths also resulted in more mois-

ture transport into the Asian continental interior. On the other hand, we found that the increased heat transport through cyclones is compensated by a decreased fraction of blocking under early Eocene conditions. Over the Southern Hemisphere, we found a decrease in mid-latitude cyclone numbers, which is connected to the decrease in temperature gradient between polar and subpolar surface water due to the lack of the ACC. Our results suggest, that the decrease in southern AHT infers the increase in OHT, which is achieved by the Southern Hemisphere-driven overturning circulation in the ocean. We conclude that under early Eocene conditions the atmospheric heat transport processes are more symmetric between the hemispheres than in the pre-industrial climate. This is achieved through air-sea-land interactions, where the pealoegeography has an important role in forming the large scale circulation both in the atmosphere and in the ocean. The next step of this research is the investigation of early Eocene cyclones in a high CO_2 simulation, which is representing the paleo conditions more accurately. Our previous analysis (Kelemen et al., 2023) showed a slight increase in transient eddy heat transport in high CO_2 simulations. Thus, we are interested to see if this is achieved through more frequent cyclones or by more heat transport per cyclone, through the warmer and moister atmosphere of the EECO climate.

Appendix A: Blocking calculation

The applied hybrid blocking index evaluates the geopotential height at 500 hPa. This hybrid index combines the gradient approach by Davini et al. (2012) with an anomaly approach based on Barriopedro et al. (2010) which we modified as described in Lohmann et al. (2024): in case of blocking the geopotential height has to exceed the climatological mean by one standard deviation. The mean value and standard deviation were calculated for each calendar day and grid cell. A 91 d window centred around the day of interest was applied for the calculation of the mean and standard deviation to smooth the yearly cycle. The climatological mean of geopotential height refers to a 31-year running window to consider changes in the mean geopotential height related to changes in global mean temperature.

In the first step, both components of the hybrid index were calculated independently. To combine both, blocked areas were checked for a joint area of at least 1.5×10^5 km^2. If this threshold was exceeded, the full area detected by the anomaly approach was counted as instantaneous block. Next, a spatio-temporal filtering was applied. The instantaneous block was finally counted as block if the block persists for at least five days, covers at least 15° in longitude and 1.5×10^6 km^2 in space. The blocking climatologies were calculated with the 2D-Blocking Plugin (Richling, 2020) from the Free Evaluation System Framework (Freva) (Kadow et al., 2021). The geopotential height fields were remapped to a $2.5° \times 2.5°$ grid, since this spatial resolution is the default setting of the 2D-Blocking Plugin (Richling, 2020) and a common resolution for blocking calculation (e.g. in Davini et al., 2012). Remapping to one resolution simplifies processing and comparing several datasets with different resolution. It does not reduce the blocking sensitivity as that is connected to the original simulation resolution.

Code and data availability. The DeepMIP CESM1.2 simulations are available by following the instructions at https://www.deepmip.org/data-eocene/ (last access: March 2026) and the restart files at https://doi.org/10.5281/zenodo.2642535 (Zhu et al., 2024). The atmosphere-only simulation data used for this study is available at https://doi.org/10.5281/zenodo.17246902 (Kelemen, 2025).

Author contributions. Conceptualization and Investigation: FDK, Data curation: FDK, JZ, Formal analysis: FDK, RL, Funding acquisition: BA. All authors contributed to the writing, reviewing and editing of the manuscript.

Competing interests. The contact author has declared that none of the authors has any competing interests.

Disclaimer. Publisher's note: Copernicus Publications remains neutral with regard to jurisdictional claims made in the text, published maps, institutional affiliations, or any other geographical representation in this paper. The authors bear the ultimate responsibility for providing appropriate place names. Views expressed in the text are those of the authors and do not necessarily reflect the views of the publisher.

Acknowledgements. This research was funded through the VeWA consortium (Past Warm Periods as Natural Analogues of our high-CO_2 Climate Future) by the LOEWE programme of the Hessen Ministry of Higher Education, Research and the Arts, Germany. FDK and BA acknowledges support from Hessen Ministry of Higher Education, Research and the Arts (Hessisches Ministerium für Wissenschaft und Kunst, Grant 67). This work used resources of the Deutsches Klimarechenzentrum (DKRZ) granted by its Scientific Steering Committee (WLA) under project ID1346. The CESM project is supported primarily by the National Science Foundation (NSF). This material is based upon work supported by the National Center for Atmospheric Research (NCAR), which is a major facility sponsored by the NSF under Cooperative Agreement No. 1852977.

Financial support. This research has been supported by the Hessisches Ministerium für Wissenschaft und Kunst (grant no. 67), the Deutsches Klimarechenzentrum (grant no. ID1346), and the National Center for Atmospheric Research (grant no. 1852977).

This open-access publication was funded by Goethe University Frankfurt.

Review statement. This paper was edited by Yannick Donnadieu and reviewed by two anonymous referees.

References

Agustsdottir, A. M., Barron, E. J., Bice, K. L., Colarusso, L. A., Cookman, J. L., Cosgrove, B. A., De Lurio, J. L., Dutton, J. F., Frakes, B. J., Frakes, L. A., Moy, C. J., Olszewski, T. D., Pancost, R. D., Poulsen, C. J., Ruffner, C. M., Sheldon, D. G., and White, T. S.: Storm activity in ancient climates 1. Sensitivity of severe storms to climate forcing factors on geologic timescales, Journal of Geophysical Research Atmospheres, 104, 27277–27293, 1999.

Akhmetiev, M. A., Zaporozhets, N. I., Benyamovskiy, V. N., Aleksandrova, G. N., Iakovleva, A. I., and Oreshkina, T. V.: The Paleogene History Of The Western Siberian Seaway-A Connection Of The Peri-Tethys To The Arctic Ocean, Austrian Journal of Earth Sciences, 105, https://www.geologie.or.at/images/OEGG/geol-ges/mitteilungen/mitt-105-1.html (last access: March 2026), 2012.

Barriopedro, D., García-Herrera, R., and Trigo, R. M.: Application of blocking diagnosis methods to General Circulation Models. Part I: a novel detection scheme, Clim. Dynam., 35, 1373–1391, https://doi.org/10.1007/s00382-010-0767-5, 2010.

Cenozoic CO_2 Proxy Integration Project (CenCO2PIP) Consortium, Hönisch, B., Royer, D. L., Breecker, D. O., Polissar, P. J., Bowen, G. J., Henehan, M. J., Cui, Y., Steinthorsdottir, M., McElwain, J. C., Kohn, M. J., Pearson, A., Phelps, S. R., Uno, K. T., Ridgwell, A., Anagnostou, E., Austermann, J., Badger, M. P. S., Barclay, R. S., Bijl, P. K., Chalk, T. B., Scotese, C. R., de la Vega, E., DeConto, R. M., Dyez, K. A., Ferrini, V., Franks, P. J., Giulivi, C. F., Gutjahr, M., Harper, D. T., Haynes, L. L., Huber, M., Snell, K. E., Keisling, B. A., Konrad, W., Lowenstein, T. K., Malinverno, A., Guillermic, M., Mejía, L. M., Milligan, J. N., Morton, J. J., Nordt, L., Whiteford, R., Roth-Nebelsick, A., Rugenstein, J. K. C., Schaller, M. F., Sheldon, N. D., Sosdian, S., Wilkes, E. B., Witkowski, C. R., Zhang, Y. G., Anderson, L., Beerling, D. J., Bolton, C., Cerling, T. E., Cotton, J. M., Da, J., Ekart, D. D., Foster, G. F., Greenwood, D. R., Hyland, E. G., Jagniecki, E. A., Jasper, J. P., Kowalczyk, J. B., Kunzmann, L., Kürschner, W. M., Lawrence, C. E., Lear, C. H., Martínez-Botí, M. A., Maxbauer, D. P., Montagna, P., Naafs, B. D. A., Rae, J. W. B., Raitzsch, M., Retallack, G. J., Ring, S. J., Seki, O., Sepúlveda, J., Sinha, A., Tesfamichael, T. F., Tripati, A., van der Burgh, J., Yu, J., Zachos, J. C., and Zhang, L.: Toward a Cenozoic history of atmospheric CO_2, Science, 382, eadi5177, https://doi.org/10.1126/science.adi5177, 2023.

Davini, P., Cagnazzo, C., Gualdi, S., and Navarra, A.: Bidimensional diagnostics, variability, and trends of Northern Hemisphere blocking, J. Climate, 25, 6496–6509, https://doi.org/10.1175/JCLI-D-12-00032.1, 2012.

Evans, D., Sagoo, N., Renema, W., Cotton, L. J., Müller, W., Todd, J. A., Saraswati, P. K., Stassen, P., Ziegler, M., Pearson, P. N., Valdes, P. J., and Affek, H. P.: Eocene greenhouse climate revealed by coupled clumped isotope-Mg/Ca thermometry, Proceedings of the National Academy of Sciences, 115, 1174–1179, 2018.

Frieling, J., Iakovleva, A. I., Reichart, G.-J., Aleksandrova, G. N., Gnibidenko, Z. N., Schouten, S., and Sluijs, A.: Paleocene–Eocene warming and biotic response in the epicontinental West Siberian Sea, Geology, 42, 767–770, 2014.

Herold, N., Buzan, J., Seton, M., Goldner, A., Green, J. A. M., Müller, R. D., Markwick, P., and Huber, M.: A suite of early Eocene (∼ 55 Ma) climate model boundary conditions, Geosci. Model Dev., 7, 2077–2090, https://doi.org/10.5194/gmd-7-2077-2014, 2014.

Inglis, G. N., Bragg, F., Burls, N. J., Cramwinckel, M. J., Evans, D., Foster, G. L., Huber, M., Lunt, D. J., Siler, N., Steinig, S., Tierney, J. E., Wilkinson, R., Anagnostou, E., de Boer, A. M., Dunkley Jones, T., Edgar, K. M., Hollis, C. J., Hutchinson, D. K., and Pancost, R. D.: Global mean surface temperature and climate sensitivity of the early Eocene Climatic Optimum (EECO), Paleocene–Eocene Thermal Maximum (PETM), and latest Paleocene, Clim. Past, 16, 1953–1968, https://doi.org/10.5194/cp-16-1953-2020, 2020.

Kadow, C., Illing, S., Lucio-Eceiza, E. E., Bergemann, M., Ramadoss, M., Sommer, P. S., Kunst, O., Schartner, T., Pankatz, K., Grieger, J., Schuster, M., Richling, A., Thiemann, H., Kirchner, I., Rust, H. W., Ludwig, T., Cubasch, U., and Ulbrich, U.: Introduction to Freva – a Free Evaluation System Framework for earth system modeling, J. Open Res. Software, 9, 13, https://doi.org/10.5334/jors.253, 2021.

Kelemen, F. D.: CESM1.2 simulation data for the paper "Role of paleogeography on large-scale circulation during the early Eocene", Zenodo [data set], https://doi.org/10.5281/zenodo.17246902, 2025.

Kelemen, F. D., Bartholy, J., and Pongracz, R.: Multivariable cyclone analysis in the Mediterranean region, Időjárás, 119, 159–184, 2015.

Kelemen, F. D., Steinig, S., de Boer, A., Zhu, J., Chan, W.-L., Niezgodzki, I., Hutchinson, D. K., Knorr, G., Abe-Ouchi, A., and Ahrens, B.: Meridional heat transport in the DeepMIP Eocene ensemble: Non-CO_2 and CO_2 effects, Paleoceanography and Paleoclimatology, 38, e2022PA004607, https://doi.org/10.1029/2022PA004607, 2023.

Lohmann, R., Purr, C., and Ahrens, B.: Northern Hemisphere atmospheric blocking in CMIP6 climate projections using a hybrid index, J. Climate, https://doi.org/10.1175/JCLI-D-23-0589.1, 2024.

Lunt, D. J., Huber, M., Anagnostou, E., Baatsen, M. L. J., Caballero, R., DeConto, R., Dijkstra, H. A., Donnadieu, Y., Evans, D., Feng, R., Foster, G. L., Gasson, E., von der Heydt, A. S., Hollis, C. J., Inglis, G. N., Jones, S. M., Kiehl, J., Kirtland Turner, S., Korty, R. L., Kozdon, R., Krishnan, S., Ladant, J.-B., Langebroek, P., Lear, C. H., LeGrande, A. N., Littler, K., Markwick, P., Otto-Bliesner, B., Pearson, P., Poulsen, C. J., Salzmann, U., Shields, C., Snell, K., Stärz, M., Super, J., Tabor, C., Tierney, J. E., Tourte, G. J. L., Tripati, A., Upchurch, G. R., Wade, B. S., Wing, S. L., Winguth, A. M. E., Wright, N. M., Zachos, J. C., and Zeebe, R. E.: The DeepMIP contribution to PMIP4: experimental design for model simulations of the EECO, PETM, and pre-PETM (version 1.0), Geosci. Model Dev., 10, 889–901, https://doi.org/10.5194/gmd-10-889-2017, 2017.

Lunt, D. J., Bragg, F., Chan, W.-L., Hutchinson, D. K., Ladant, J.-B., Morozova, P., Niezgodzki, I., Steinig, S., Zhang, Z., Zhu, J., Abe-Ouchi, A., Anagnostou, E., de Boer, A. M., Coxall, H. K., Donnadieu, Y., Foster, G., Inglis, G. N., Knorr, G., Langebroek, P. M., Lear, C. H., Lohmann, G., Poulsen, C. J., Sepul-

chre, P., Tierney, J. E., Valdes, P. J., Volodin, E. M., Dunkley Jones, T., Hollis, C. J., Huber, M., and Otto-Bliesner, B. L.: DeepMIP: model intercomparison of early Eocene climatic optimum (EECO) large-scale climate features and comparison with proxy data, Clim. Past, 17, 203–227, https://doi.org/10.5194/cp-17-203-2021, 2021.

Mei, J., Wen, X., Yu, F., and Yan, Y.: The C-shaped landmass: A key driver of monsoon formation, Geophysical Research Letters, 52, e2024GL112127, https://doi.org/10.1029/2024GL112127, 2025.

Ramstein, G.: Climates of the earth and cryosphere evolution, Surveys in Geophysics, 32, 329–350, 2011.

Richling, A.: 2D-Blocking, Tech. rep., FU Berlin, https://gitlab.met.fu-berlin.de/tools4freva/blocking_2D (last access: March 2026), 2020.

Scher, H. D., Whittaker, J. M., Williams, S. E., Latimer, J. C., Kordesch, W. E., and Delaney, M. L.: Onset of Antarctic Circumpolar Current 30 million years ago as Tasmanian Gateway aligned with westerlies, Nature, 523, 580–583, 2015.

Shaw, T. A., Miyawaki, O., and Donohoe, A.: Stormier Southern Hemisphere induced by topography and ocean circulation, Proceedings of the National Academy of Sciences, 119, e2123512119, https://doi.org/10.1073/pnas.2123512119, 2022.

Shellito, C. J., Lamarque, J.-F., and Sloan, L. C.: Early Eocene Arctic climate sensitivity to pCO2 and basin geography, Geophysical Research Letters, 36, https://doi.org/10.1029/2009GL037248, 2009.

Wang, P.: Cenozoic Deformation and the History of Sea-Land Interactions in Asia, in: Continent-Ocean Interactions Within East Asian Marginal Seas, edited by: Clift, P., Kuhnt, W. and Hayes, D., American Geophysical Union (AGU), 1–22, ISBN 9781118666067, https://doi.org/10.1029/149GM01, 2004.

Zhang, Y., de Boer, A. M., Lunt, D. J., Hutchinson, D. K., Ross, P., van de Flierdt, T., Sexton, P., Coxall, H. K., Steinig, S., Ladant, J.-B., Zhu, J., Donnadieu, Y., Zhang, Z., Chan, W.-L., Abe-Ouchi, A., Niezgodzki, I., Lohmann, G., Knorr, G., Poulsen, C. J., and Huber, M.: Early Eocene ocean meridional overturning circulation: The roles of atmospheric forcing and strait geometry, Paleoceanography and Paleoclimatology, 37, e2021PA004329, https://doi.org/10.1029/2021PA004329, 2022.

Zhu, J., Poulsen, C. J., and Tierney, J. E.: Simulation of Eocene extreme warmth and high climate sensitivity through cloud feedbacks, Science Advances, 5, eaax1874, https://doi.org/10.1126/sciadv.aax1874, 2019.

Zhu, J., Poulsen, C. J., and Tierney, J. E.: CESM1.2 simulation data for “Simulation of Eocene extreme warmth and high climate sensitivity through cloud feedbacks”, Zenodo [data set], https://doi.org/10.5281/zenodo.2642535, 2024.